communications earth & environment

Article

A Nature Portfolio journal

Article in Press

https://doi.org/10.1038/s43247-026-04197-1

Large intraplate earthquakes on an extinct oceanic plate reveal fracture zone reactivation

Check for updates

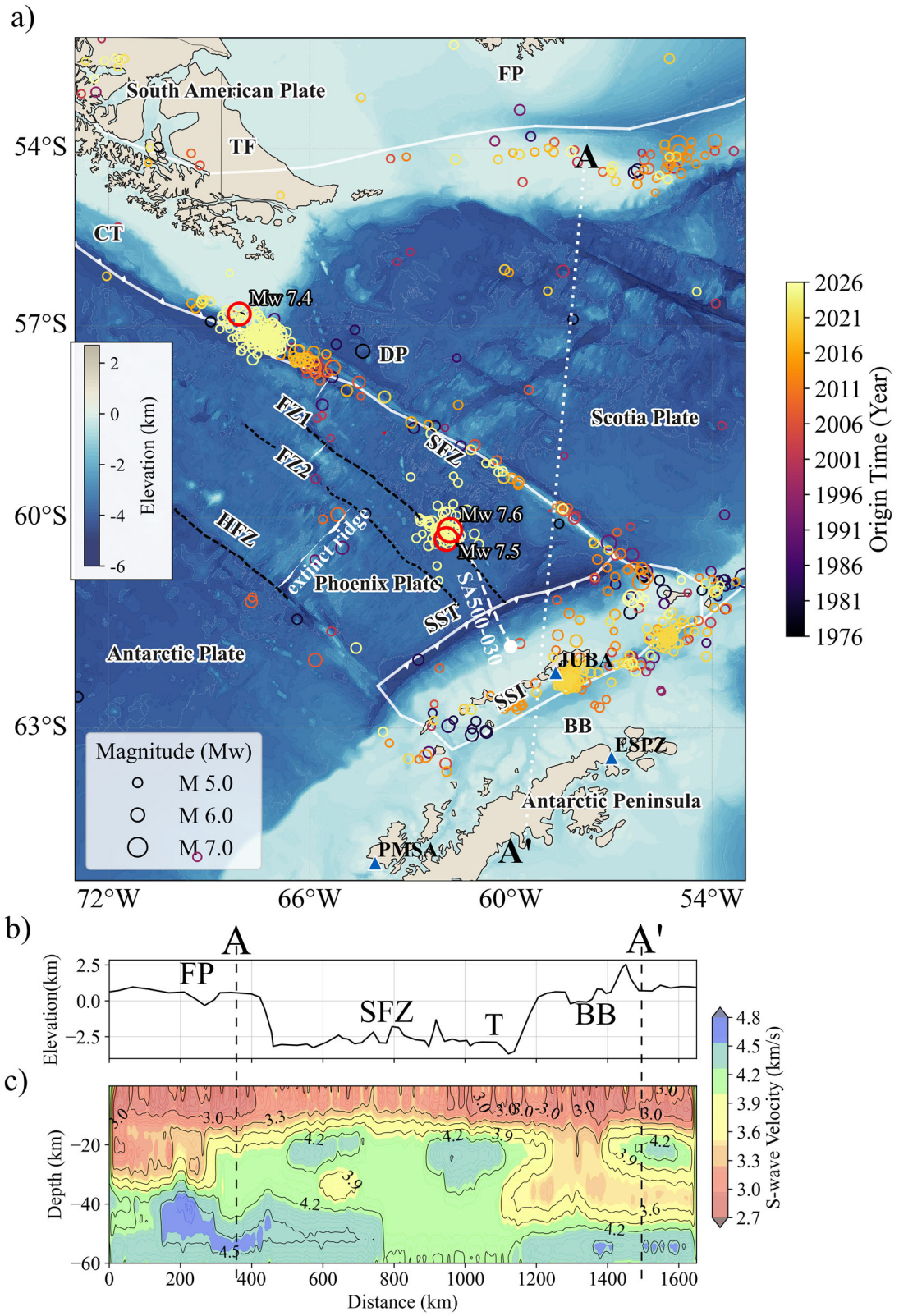
Emanuele Lodolo[1] ✉, Alessandro Vuan[1], Alina Polonia[2], Marco Menichetti[3], Andrea Magrin[1] & Marco Santulin[1]

Oceanic transform faults are often considered tectonically inactive once plate motion ceases. However, their long-term mechanical behavior and role in intraplate deformation remain poorly understood. Here, we analyze two earthquakes of Mw 7.5 and Mw 7.6 that occurred about 15 km apart in 2025 within the Phoenix Plate, along a structure spatially consistent with a former oceanic transform fault in the Drake Passage region. These events demonstrate that such structures retain lithospheric-scale mechanical integrity and can be reactivated under present-day stress conditions. We propose here that inherited fault geometry and regional far-field stresses associated with Scotia–Antarctic plate interactions, collectively promote strain localization on these supposed fossil structures. Our results indicate that cessation of plate-boundary activity does not imply mechanical quiescence and that oceanic fracture zones represent long-lived zones of intraplate weakness capable of both hosting large-magnitude earthquakes and favoring magma emplacement, as shown by a seismic profile crossing the fracture zone near the earthquake locations. We suggest that this structure acts as a lithosphere-scale tear fault on the subducting Phoenix Plate beneath the South Shetland continental block. This behavior has implications for the mechanical evolution of oceanic lithosphere and the interpretation of intraplate seismicity in regions of extinct plate boundaries.

Large intraplate earthquakes within inactive oceanic plates are quite rare and provide valuable insight into the persistence of rheological heterogeneities in the oceanic lithosphere. Former transform faults and fracture zones are recognized as structures of crustal and upper mantle weakness that may be reactivated under changing stress regimes. However, the long-term mechanical fate of oceanic transform faults and fracture zones following spreading ridge extinction remains an open question. Two earthquakes of magnitude Mw 7.5 and Mw 7.6 occurred a few months apart in 2025 within the now-extinct Phoenix Plate in the Drake Passage region (Fig. 1), raising fundamental questions about the long-term inheritance of inactive plate boundaries. These events nucleated along Cenozoic lithospheric structure formed during the spreading history of the Phoenix Plate. The progressive slowdown of Phoenix Plate subduction beneath the South Shetland Trench along the northern Antarctic Peninsula region[1] has resulted in a complex stress field driven by slab rollback, plate bending, and slab detachment processes.

In this study, we analyze two seismic events that occurred in the Drake Passage to explain the role of fracture zones in triggering large-magnitude earthquakes. The results indicate that fossil lithospheric discontinuities may remain mechanically weak and susceptible to reactivation under suitable stress conditions, even millions of years after spreading cessation, due to the brittle behavior of cooled oceanic crust. According to previous studies based on P-wave receiver function[2], the fracture zone hosting the two intraplate earthquakes functions as a tear fault within the subducting Phoenix slab, accommodating differential slab motion and contributing to segmentation of the South Shetland subduction system. This interpretation connects intraplate seismicity to ongoing slab-scale deformation processes and highlights the influence of inherited oceanic plate architecture on deformation during subduction termination and slab fragmentation. A seismic profile crossing obliquely the fracture zone near the earthquake epicenters, where significant magma emplacement occurs, supports this view. Interpreting these earthquakes as evidence of tear-fault activity offers new insight into the ability of fossil plate structures to localize large-magnitude seismicity long after spreading and transform motion have ended.

[1]Istituto Nazionale di Oceanografia e di Geofisica Sperimentale - OGS, Trieste, Italy. [2]Istituto di Scienze Marine - CNR-ISMAR, Bologna, Italy. [3]Dipartimento di Scienze Pure ed Applicate, Università di Urbino, Urbino, Italy. ✉e-mail: elodolo@ogs.it



Geologic and tectonic context of the Phoenix Plate

The Phoenix Plate, located in the Drake Passage, is a geologically complex region where the South America, Antarctic, and Scotia plates meet (see Fig. 1). The opening of the Drake Passage marked the final phase of the Gondwana supercontinent breakup, with the separation of the southern tip of South America from the northern Antarctic Peninsula, leading to the development of the oceanic Scotia Sea[3–6]. The Phoenix Plate originated at the Phoenix–Antarctic ridge, where seafloor spreading occurred from the Jurassic through the early Cenozoic[7,8]. During this period, the ridge segments and their associated transform faults of the Phoenix Plate progressively collided south-eastward and subducted beneath the western margin of the Antarctic Peninsula. Convergence rates decreased over time as regional

Fig. 1 | Map of study area, earthquake distribution, and tomographic cross-section. a Hill-shaded GEBCO bathymetry (https://www.gebco.net/data-products-gridded-bathymetry-data/gebco2026-grid) of the Drake Passage region underlies the epicentral distribution of USGS earthquakes recorded and located between 1976 and 2026. Event magnitudes are indicated by the diameter of unfilled circles, while the edge color of each symbol denotes origin time. Labels are as follows: FP Falkland Plateau, CT Chilean Trench, SFZ Shackleton Fracture Zone, FZ1 and FZ2 fracture zones of the Phoenix Plate (corresponding to FZE and FZD, respectively, as labeled by Barker, 1982), HFZ Hero Fracture Zone, SST South Shetland Trench, SSI South Shetland Islands, TF Tierra del Fuego, BB Bransfield Basin, DP Drake Passage. JUBA, ESPZ, and PMSA (blue triangles) indicate the seismic stations used in this study to relocate earthquakes. **b** Bathymetry projected along the A–A' transect in **a**. **c** Shear-wave velocity structure along the A–A' transect across the Drake Passage. S-wave velocities are derived from color-matched surface wave tomographic inversion[55], with contour intervals of 0.3 km/s and labeled reference levels at 2.7–4.8 km/s. The section shows strong lateral and vertical velocity contrasts associated with crustal thinning, fault-controlled domains, and the transition from continental to oceanic lithosphere.

plate reorganizations altered the relative motions between the Phoenix, Antarctic, and South American plates[8,9]. This timing coincides with the cessation of spreading at the Antarctic–Phoenix[8,10], after which the Phoenix Plate was incorporated into the Antarctic Plate due to a lack of relative motion across that boundary, rendering the plate tectonically extinct. Remnants of the Phoenix Plate are now bounded to the south-west by the Hero Fracture Zone and to the north-east by the Shackleton Fracture Zone (SFZ), a NW-SE trending fracture zone that extends over 800 km from the southernmost Chilean trench to the eastern end of the South Shetland Trench[11–14]. This fracture zone now juxtaposes two fossil spreading centers, the West Scotia ridge to the east (extinct at ~10 Myr[15,16]) and the former Phoenix-Antarctic ridge to the west.

Seismicity and focal mechanisms indicate that the SFZ is an active, left-lateral transpressive fault zone that, together with the South Scotia Ridge, accommodates relative motion between the Scotia and Antarctic plates[12,15–18]. The margin of the South Shetland subduction zone, north of the Hero Fracture Zone, is generally considered to be still weakly active. In this area, the Phoenix Plate is interpreted to continue subducting beneath the South Shetland Islands, as suggested by trench morphology, compressional structures, and some seismicity[1]. In contrast, the segment south of the Hero Fracture Zone is commonly regarded as inactive or fossil, because most of the Phoenix Plate has already been consumed and plate convergence with the Antarctic Plate has largely ceased. As subduction progressively decreased, the remnant subducted slab continued to roll back, generating extensional stresses in the overriding plate and contributing to the opening of the Bransfield Basin as a back-arc rift[19,20]. A large amount of geophysical data acquired mostly in the 1990s, geodetic surveys and the seismicity indicate that the Bransfield Basin is undergoing active extension, with a rate of ~10 mm/yr directed NW-SE, orthogonal to the strait's strike[21].

Recent seismicity in the Drake Passage

The Drake Passage region experienced three powerful earthquakes in 2025, each with a magnitude greater than 7.4. These are exceptionally strong earthquakes for an area where the plates move slowly: the Antarctic and Scotia plates move at approximately 6–9 mm/yr, as determined by global plate motion models and geodetic data[22–24]. This motion is mainly accommodated along the left-lateral South Scotia Ridge and the SFZ. A Mw 7.4 earthquake on May 2 occurred about 120 km off the southern tip of South America near Tierra del Fuego, at the intersection of the SFZ and the southern Chilean Trench (see Fig. 1). The predominantly compressional mechanisms with relatively steep dips, along with the clustering of aftershocks in the lower crust and upper mantle, support a composite rupture in which slip was distributed across multiple fault segments[25]. The Mw 7.5 earthquake on August 22 and Mw 7.6 on October 10, which occurred very close to each other (about 15 km apart, according to the Unites States Geological Survey - USGS), took place about 500 km south of the May 2 event. This level of earthquake activity is highly unusual for this region. The two earthquakes in August and October are similar in magnitude and focal mechanism. Both exhibit strike-slip motion with very similar nodal planes, possibly associated with either NNE-trending right-lateral faults or WNW-trending left-lateral faults[26]. Because the region is so remote, there is almost no data from within 250 km, with the closest stations being those of the Antarctic Seismographic Argentinean Italian Network – ASAIN[27]. Small earthquakes, such as most aftershocks, are largely undetected, and these have significant uncertainties in location; as a result, aftershock patterns are not very useful for accurate analysis. Due to these limitations, advanced methods were used to improve earthquake detection and expand the number of identifiable events (see details in "Methods"). Starting with the 49 earthquakes listed in the USGS catalog (see Table 1 in the Supplementary Information), we detect approximately two hundred additional events that occurred between August and the end of November 2025 (Fig. 2). The temporal evolution of the sequence (Fig. 2c) shows that seismicity remained persistently elevated for approximately five months, punctuated by two events of comparable magnitude, Mw 7.5 and Mw 7.6, separated by ~49 days. Rather than a single mainshock followed by a decaying aftershock sequence, this pattern is more consistent with an earthquake doublet: two closely spaced, similarly sized ruptures, each generating its own local aftershock cluster, with the second event occurring while the first sequence was still active.

Geometric analysis of fracture zone FZ1 (Fig. 3) indicates an azimuth of ~310°, whereas the focal mechanisms of the two main shocks yield strike orientations near 285°. A magnitude weighted Principal Component Analysis (PCA) of the spatial distribution of the augmented catalog identifies a principal axis that aligns closely with the strike directions of the Global Centroid Moment Tensor (GCMT) focal mechanisms. Despite the potential for significant uncertainties arising from the azimuthal station gap and horizontal mislocations on the order of 10–15 km (as suggested by discrepancies between USGS and ASAIN regional locations), the GCMT solutions remain stable across events ranging from Mw 5 to Mw 7.6 (Fig. 3c). Following the 10 October earthquake (Fig. 3b), aftershocks align more closely with the FZ1, and the PCA axis exhibits a slight rotation, reflecting the increased number of detections along FZ1. This suggests that the fracture zone visible in bathymetry may not fully control the orientation of the main rupture propagation. The active rupture plane may select a different orientation due to stress reorganization from dominant deeper lithospheric processes (see Table 2 in the Supplementary Information) or inherited weak zones.

The back-projection of P-wave coherence maxima (see details in Methods) identifies the part of each rupture radiating the most coherent high-frequency energy, a proxy for the direction of fastest/largest slip propagation. The two events differ not only in azimuth but in rupture mode (Fig. S1a, S1b). The August mainshock directivity appears to resolve into two phases: an initial phase directed ENE, followed, after peak coherence is reached, by a second phase directed SE. The October event, by contrast, appears purely bilateral, with coherent energy directed simultaneously toward WNW and ESE. The two ruptures also differ in the timing of peak coherence release: in August, high coherence is reached almost instantaneously after nucleation, whereas in October it is delayed by approximately 15 s (Fig. S2). The 95th-percentile envelope of aftershock distance grows with time as a shallow power law for both sequences ($r_{95} \propto t^{0.193}$ for 22 August, $r_{95} \propto t^{0.141}$ for 10 October) (Fig. S1d). The two sequences differ in a specific and informative way: the October envelope starts substantially wider ($r_{95} \approx 29$ km within the first ~15 min, versus ≈16 km for the August event) but grows more slowly thereafter (exponent 0.141 vs. 0.193), while the August envelope starts more tightly confined near the epicenter and expands proportionally faster. By 49 days, the two envelopes converge toward comparable radii (81.5 km vs. 96.4 km). A 49-day, 10–15 km-scale triggering relationship between two M 7.5-class events is fast and close by intraplate standards, well inside the canonical doublet definition[28] comparable in timing to the stress-transfer doublet documented by Ammon

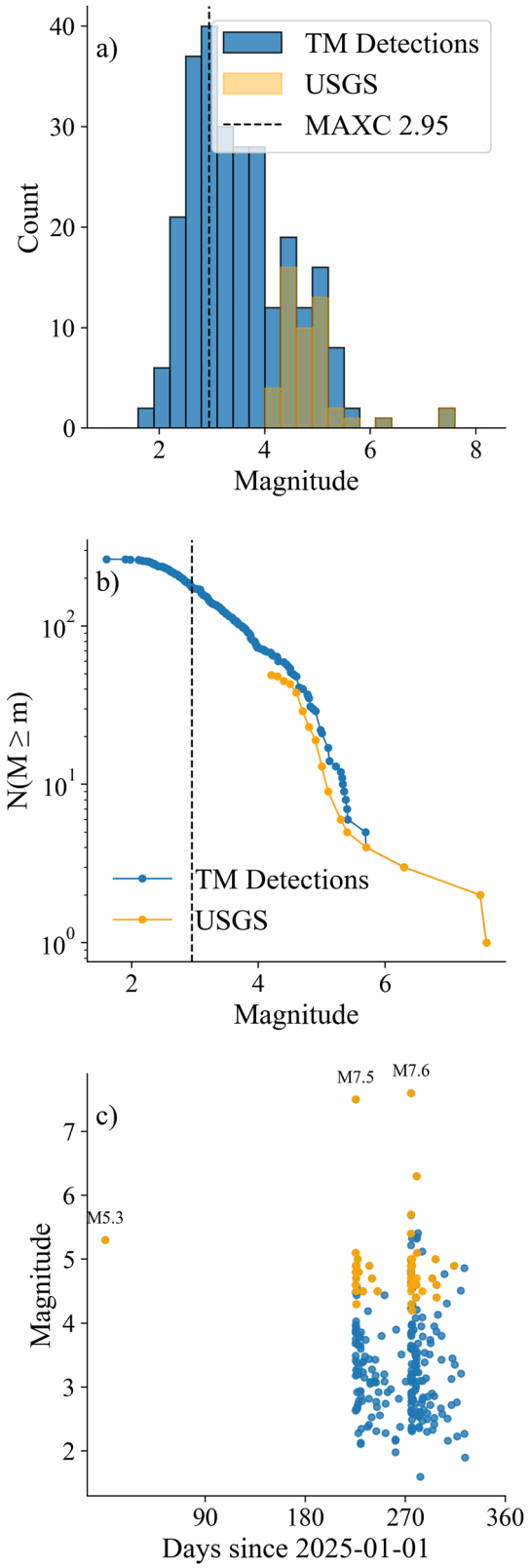


Fig. 2 | Magnitude-completeness assessment using local and USGS earthquake catalogs. a Histogram of local (blue) and USGS (orange) magnitudes illustrating the relative detection performance of template matching (TM) and showing completeness estimates from the maximum curvature method (MAXC). **b** Cumulative frequency–magnitude distribution (FMD) for both catalogs plotted on a semi-logarithmic scale; the MAXC completeness threshold (Mc) is indicated along the corresponding vertical line. **c** Time–magnitude evolution of local and USGS events expressed as days since the first local detection, highlighting differences in sensitivity and temporal coverage.

et al[29]. but markedly closer in space, and well within the single-rupture-length triggering distance established by King et al.[30] and Stein[31] given the expected ~100 km rupture length for an event of this magnitude[32].

The combination of different directivity azimuths, structurally different aftershock migration behavior, and a host structure with multiple parallel candidate faults right where the events occurred, favors an *en-echelon*, multi-strand interpretation over a single fault reactivating twice: most plausibly, the 22 August rupture broke one strand (or a stepped set of strands) trending close to FZ1, and the 10 October rupture, triggered by the stress change from the first event, given the 49-day gap and its proximity, broke an adjacent, sub-parallel strand with a similar local strike or segment length, hence the different propagation direction and different aftershock behavior.

Bathymetry in the earthquake area reveals the classic fabric of oceanic crust near strike-slip zones, where motion generates localized "drag" deformation near the fracture zone. The young oceanic crust formed at the spreading axis is rotated in the direction of movement, and in this case, the motion inferred from these landforms is clearly left-lateral, similar to the SFZ. The off-axis morphology of the spreading corridor between FZ1 and SFZ is generally comparable to that of fast- to intermediate-rate spreading ridges, such as the Pacific-Antarctic Ridge[33], which are dominated by linear, axis-parallel magmatic ridges and straight, sharply defined fracture zones.

Multichannel seismic reflection profile

The SA500-030 seismic line shown in Fig. 4, acquired in 1987/1988 (see details in Methods), and is very close to the earthquake epicenters and crosses obliquely both the eastern oceanic fracture zone of the former Phoenix Plate (FZ1 in Fig. 1) and the South Shetland subduction zone. The line intersects fracture zone FZ1 about 60 km south of the earthquake cluster in Fig. 3a. Fracture zone FZ1 offsets the two adjacent ridge axes of the Phoenix Plate by approximately 110 km, juxtaposing oceanic crust of different ages, as inferred from the identified magnetic anomalies: 5 C to the east and 5D to the west at this point[34]. The area where the seismic line intersects FZ1 shows a series of magma bodies that reach the sea floor with an articulated morphology over about 10 km. The thickness of the sedimentary cover progressively increases toward the South Shetland subduction trench. Here, thick trench-fill sediments cover the downgoing oceanic crust, which appears segmented by a series of normal faults, generating a horst and graben pattern. Contractional structures observed in the accretionary wedge of the South Shetland Trench may indicate active compression within the subduction complex. According to other authors[35], this compression is thought to result from the northwestward movement of the South Shetland platform due to extension of the Bransfield Basin.

Discussion

Large intraplate earthquakes are relatively uncommon and pose significant challenges to our understanding of lithospheric deformation, especially when they occur within long-abandoned oceanic plates. The two recent earthquakes of magnitude 7.5 and 7.6 recorded within the Phoenix Plate, far from active plate boundaries, highlight the potential for significant strain release in regions considered tectonically inactive.

Despite the cessation of spreading and the slowdown of subduction, the oceanic seafloor of the Phoenix Plate retains a strong inherited lithospheric architecture, preserved today by clearly evident fossil spreading centers and fracture zones, as shown on available bathymetric maps[34]. The two intraplate earthquakes that occurred along the eastern fracture zone of the Phoenix Plate (i.e., FZ1 in Fig. 1) indicate reactivation of a long-lived zone of mechanical weakness. Ongoing Scotia–Antarctica relative motion, combined with slab-related processes along nearby subduction zones and possible slab detachment beneath the South Shetland Islands, continues to

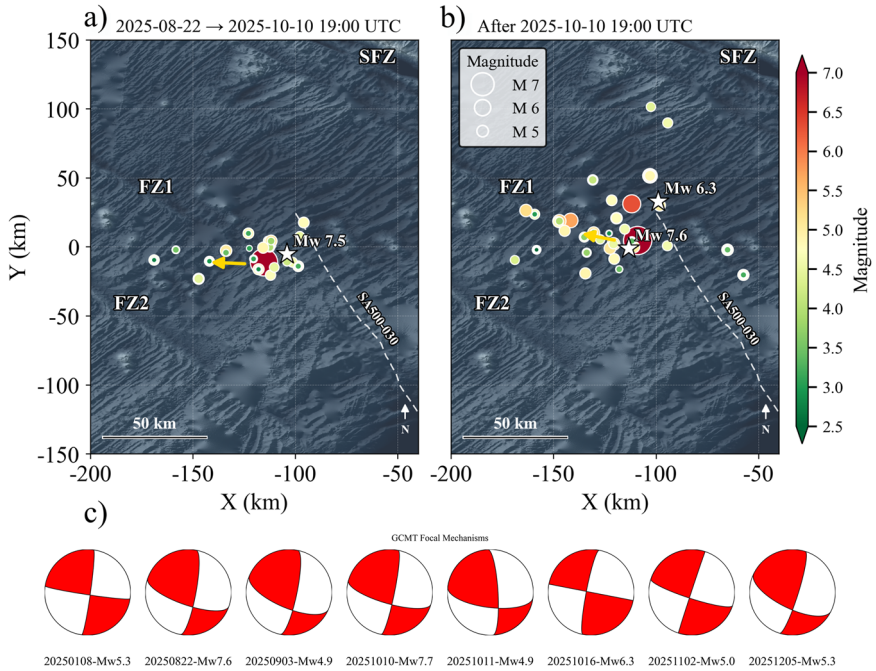


Fig. 3 | Seafloor morphology, seismicity, and temporal evolution of earthquake clustering. **a** Earthquakes recorded between 22 August and 10 October 2025 in the Phoenix Plate are plotted over hill-shaded bathymetry[34]. Event magnitudes are represented by the diameter of unfilled circles, with small filled dots marking epicenters; colors indicate relative magnitude classes. The Shackleton Fracture Zone (SFZ), and fault zones (FZ1, FZ2) are indicated. The seismic line SA500-030 is also shown for spatial context. **b** Seismicity after 10 October 2025, highlighting persistent activity distributed along the same structural domain FZ1. In both panels, areas of highest event concentration coincide with density ridges derived from kernel density estimates. Principal cluster orientations are shown by weighted Principal Component Analysis (PCA) yellow arrows, illustrating the dominant axis of spatial elongation. White star symbols denote OGS-relocated events with magnitudes ≥M 6. **c** Fault-plane solutions for the two largest and other earthquakes (indicated by their date and time of occurrence) based on Global Centroid Moment Tensor – GCMT (see Table 2 in the Supplementary Information).

impose stresses within the remnant Phoenix lithosphere[36,37]. The occurrence of two large events in close temporal and spatial proximity suggests stress redistribution, where the first earthquake may have increased stress on adjacent segments of the fracture zone, triggering the second event. If the maximum horizontal compressive stress is oriented obliquely to the fracture zone, it can promote strike-slip or oblique-slip motion. From a geodynamic perspective, these earthquakes show that fossil oceanic plates are not entirely aseismic but can host significant intraplate seismicity when pre-existing structures are optimally oriented within the regional stress field. We may also assume that plate convergence, such as that along the South Shetland Trench, can partly contribute to the reactivation of FZ1, which perturbs the stress field and thus increases the likelihood of strike-slip motion along FZ1. The southern extension of FZ1, which hosted the two earthquakes, coincides with the 2020–2021 Orca earthquake swarm in the central Bransfield Basin. This major seismic event involved over 85,000 recorded earthquakes, with magnitudes up to 5.9 and 6.0, interpreted as triggered by the intrusion of 0.26–0.56 km^3 of magma off the Orca seamount at approximately 20 km depth. Deeper, clustered strike-slip earthquakes indicate magmatic intrusion at depth, while shallower normal faulting events are induced by the growth of a lateral dike extending about 20 km NE–SW[38].

Analyses of P-wave receiver functions revealed a significant 15 km tear in the subducted Phoenix slab beneath the Bransfield Basin, coinciding with the epicenter of the 2020–2021 Orca earthquake swarm[2,39]. These authors interpret the slab tear as a conduit for hot mantle flow, facilitating the magmatic underplating observed beneath the central Bransfield Basin.

Two other significant elements suggest that the fossil oceanic fracture zone FZ1 influenced the morphological and structural characteristics of the South Shetland overriding crustal block and the Bransfield Basin. The fracture zone acts as a major morphological discontinuity, dividing two sectors characterized by a narrow continental margin to the SW and a broader eastern continental shelf. Furthermore, the outcropping volcanic edifices that characterize the Bransfield Basin, which are virtually absent in its northeastern sector, suggest that FZ1 may act as a barrier to magma ascent[40].

Most reconstructions indicate that the opening of the Bransfield Basin is neither spatially uniform nor temporally constant, but occurs through segmented and asymmetric rifting. Slab discontinuities can facilitate asthenospheric upwelling through slab windows or at slab edges, leading to localized thermal anomalies in the overriding plate. These processes may explain abrupt changes in volcanic arc composition and distribution observed in segmented subduction systems. Some studies suggest that extension of the Bransfield Basin propagated from the northeastern sector to the southwest, consistent with a propagating rift model[41,42]. Based on these results, it can be hypothesized that the southern termination of FZ1, which hosted the two large earthquakes, represents a slab-scale tear fault accommodating differential motion within the subducted Phoenix lithosphere and contributing to segmentation of the South Shetland subduction system (Fig. 5). Oceanic tear faults are first-order lithospheric discontinuities that can significantly influence the tectonic evolution of the overriding plate in subduction settings. By segmenting the downgoing slab, these structures introduce strong along-strike variations in mechanical coupling at the plate interface that may propagate in the upper plate. This interpretation highlights the role of inherited plate structures in controlling deformation during the terminal phases of plate subduction and slab fragmentation. Therefore, the South Shetland subduction zone may not represent a simple near-extinct margin, but rather a zone of ongoing lithospheric reorganization, where intraplate deformation within the remnant Phoenix slab reflects the continued influence of Scotia–Antarctica relative motion.

The large intraplate earthquakes observed in the extinct Phoenix Plate share key similarities with the 25 March 1998 Mw 8.1 Balleny Islands earthquake, the largest recorded intraplate event within the Antarctic Plate, which occurred in a region of very low seismicity far from active plate boundaries[43]. This earthquake involved a ~200 km-long, shallow, east-west–trending, left-lateral strike-slip rupture, with an average slip of ~4–5 m[44]. It provides key evidence that large earthquakes can occur within oceanic plate interiors through the reactivation of inherited lithospheric structures[45]. In both the Drake and Balleny earthquake cases, large-magnitude intraplate seismicity is best explained by regional plate reorganization, including changes in relative plate motions and stress transmission, underscoring the role of inherited plate fabric in controlling deformation during major tectonic transitions.

In the Phoenix Plate, a significant feature observed along the structure FZ1 is localized magmatism, as shown by the seismic profile. This occurs because tear faults, like other major strike-slip faults, can create paths of least resistance; their deep, sub-vertical, and often long-lived nature provides channels for magma emplacement, especially in transtensional tectonic regimes. Additionally, where the faults step over, they may create small,

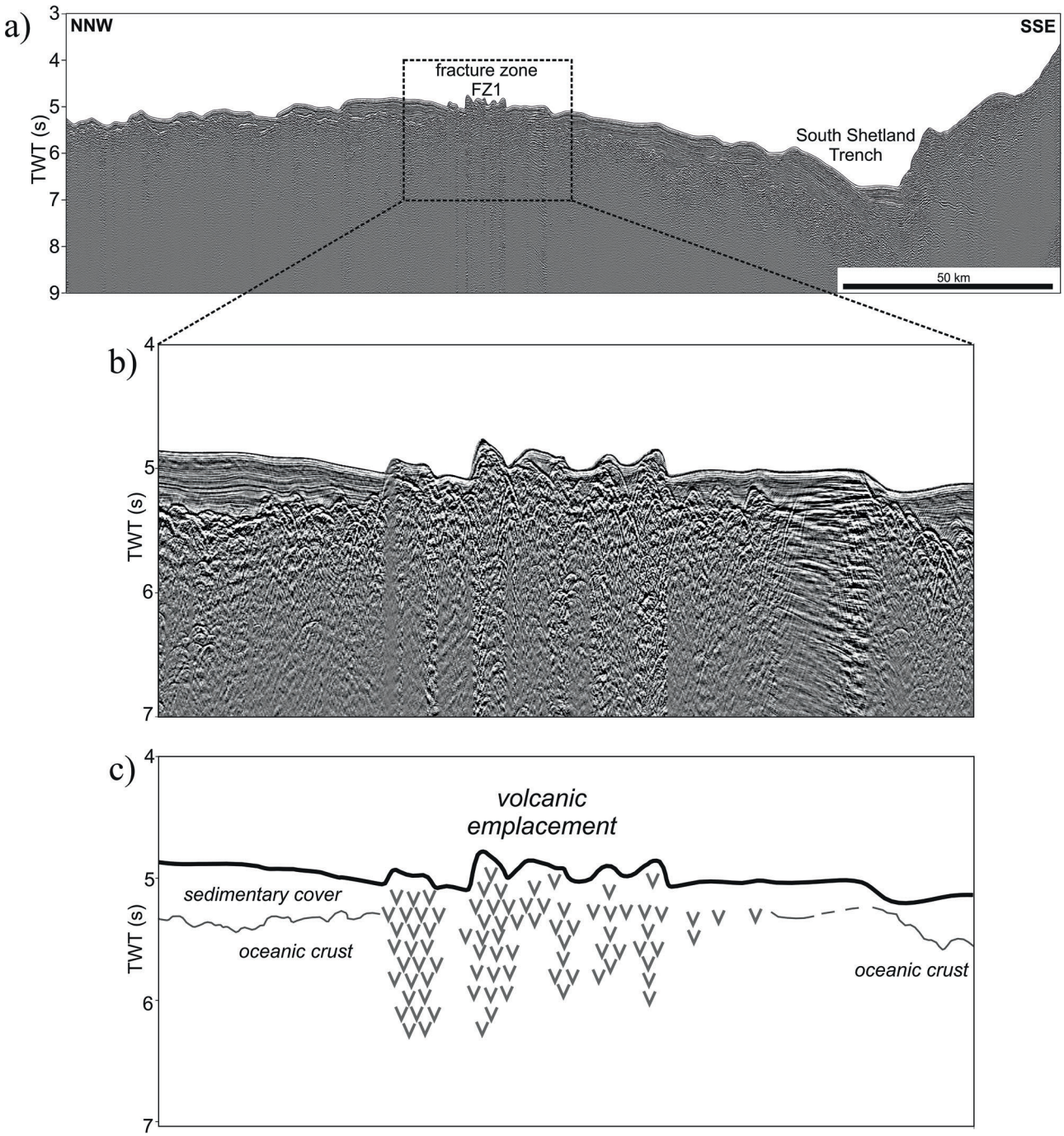


Fig. 4 | Multichannel seismic reflection profile SA500-30 crossing the oceanic fracture zone. a From NNW to SSE, the profile crosses the oceanic spreading corridor bounded by the Shackleton Fracture Zone and fracture zone FZ1, the fracture zone FZ1, the oceanic spreading corridor between the fracture zone FZ1 and fracture zone FZ2, the South Shetland Trench, and part of the South Shetland lower margin. The box in the upper panel indicates the magmatic emplacement found along the intersecting FZ1 fracture zone. **b** Part of the seismic line showing the details of the magmatic rises corresponding to the FZ1 fracture zone. **c** Simplified line drawing of **b** highlighting the presence of magmatic features. The position of line SA500-030 is shown in Fig. 1a.

confined pull-apart basins along their length, which lower the pressure on the underlying asthenosphere and trigger melting. However, it is not possible to determine whether these magmatic manifestations on the seafloor are present along the entire extent of the transform zone, as continuous bathymetric and seismic data covering this structure are lacking.

Large-scale continental transform faults associated with active volcanism are well documented in the literature. One of the most studied is the Dead Sea transform, a major left-lateral fault that accommodates strike-slip movement between the Arabian Plate (to the east) and the Sinai Sub-plate (to the west). It acts as a tear structure between the Red Sea spreading center (extension) and the Zagros collision zone (compression). Along its length, especially in its northern and southern sections, there is significant Pliocene volcanism erupted on both shoulders of the fault system, and thick sections of volcanics have accumulated along its axis[46,47]. Inherited structures within the lower plate may exert a significant control on plate dynamics, even where very old oceanic crust is involved. In the central Mediterranean Sea, the Calabrian Arc is a narrow subduction system accommodating Africa/Eurasia plate convergence and is affected by deep lithospheric fragmentation. Mechanical and numerical models suggest that Mesozoic fracture zones and transform faults control the segmentation of the subduction

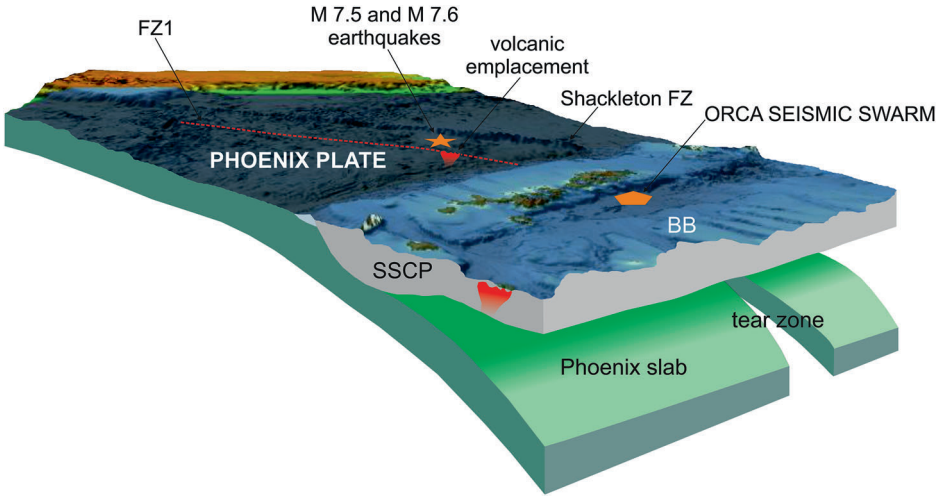


Fig. 5 | Simplified 3D scenario of the Phoenix–South Shetland subduction plate system. The discontinuity in the subduction plane caused by the FZ1 tear fault is highlighted, along which magmatic episodes have been detected. The southward extension of FZ1 intersects the Orca seismic cluster. SSCP refers to the South Shetland Islands continental platform, while BB refers to the Bransfield Basin.

system and the basement deformation associated with slab tearing[48]. Furthermore, inherited Mesozoic discontinuities, reactivated during a Quaternary extensional phase, have disrupted the subduction complex, triggering the ascent of mud and serpentinite diapirs from the lower plate mantle[49]. Structural inheritance thus represents fundamental lithospheric weakness that can directly influence the location and character of igneous activity for tens of millions of years. They act as "accommodation structures" that mediate strain transfer between crustal blocks, allowing them to move past one another even in the presence of concurrent tectonic processes.

In summary, the two 2025 Mw 7.5 and Mw 7.6 earthquakes that occurred in close spatial and temporal proximity within the Phoenix Plate demonstrate that the cessation of plate motion does not imply tectonic quiescence, and that former transform faults and fracture zones remain mechanically and rheologically active structures capable of hosting large-magnitude earthquakes long after their role as plate-boundary has ceased.

Methods

Earthquake signals analysis

The automated deep learning–based phase picker PhaseNet[50], which probabilistically identifies P and S wave onsets, was applied to the regional waveform dataset. However, for most lower-magnitude earthquakes, the signal quality is insufficient to yield robust phase picks or support reliable relocation. Therefore, we rely on hypocentral parameters from the USGS global catalog and use template matching[51]. In the Supplementary Information, we report the table of seismic events (from the USGS catalog) used by the template matching method and the table of GCMT parameters for focal solutions. To construct this enhanced catalog, we analyzed continuous recordings from the JUBA seismic station of the ASAIN Network – the nearest station to the sequence (~250 km)—spanning January to November 2025 (see Supplementary Information for details). Using only USGS-derived templates, we found no additional events preceding the first mainshock on 22 August. Nevertheless, the temporal evolution of the template-matched detections reveals important features of the seismic sequence and effectively lowers the completeness magnitude. Although earthquake locations in this remote region inevitably suffer from the absence of local stations, the expanded catalog enables improved constraints on the spatial extent of the aftershock zone and its dominant orientation. In addition, the Supplementary Information describes the potential complexities affecting the recorded seismic signals due to the relative position of the seismic station with respect to the analyzed events, as well as the methodological approach used to augment the earthquake catalog distributed by global seismic agencies. We also present representative examples of waveform recordings for the main events (Figs. S1–S3) and for some earthquakes in the augmented catalog not included in global bulletins (Figs. S4–S6).

Back-projection method

Back-projection is a beamforming technique used to image the space-time evolution of high-frequency seismic radiation during large earthquake rupture, independent of a fault-plane or slip-inversion model. Teleseismic P-wave (or PP/PKIKP) waveforms are collected from a large virtual network of globally distributed broadband stations (in this study, the GSN virtual network) and each station's waveform is time-shifted according to the predicted P-wave travel time from a trial source location/time to that station, using a 1-D reference Earth velocity model. Waveforms are stacked (summed, often after normalization) across the array for every trial point on a spatial grid around the epicenter and every time window through the rupture duration. Where the trial point and time coincide with the true, currently radiating patch of the fault, waveforms from many stations arrive coherently and stack constructively, producing high beam amplitude/coherence; elsewhere they interfere destructively. The result is a space-time map of coherent high-frequency radiation (0.05–0.25 Hz) that represents a proxy for where and when the rupture front was releasing energy, visualized as the cumulative coherence stack and as an amplitude-vs-time curve. This is the method underlying the standard EarthScope/IRIS DMC "Back-Projection" data product, built on the foundational methodology of Ishii et al.[52], later extended by Xu et al.[53] and Koper et al.[54], and it is the basis for the near-real-time summary plots that USGS and EarthScope routinely generate for large ($M \geq 7$) earthquakes.

We must remark that BP images the location of coherent high-frequency radiation, not fault slip amplitude or moment release and the coherence maximum is not necessarily the point of peak slip. Spatial resolution scales with the frequency band used and the network's geometry (azimuthal coverage, aperture). Moreover, most teleseismic BP implementations solve only for horizontal (2-D) position at a fixed and the vertical dimension of rupture is unconstrained. Apparent rupture "propagation" in BP images can be influenced by the source-receiver geometry (stations preferentially in the along-strike direction enhance apparent directivity), so directivity inferred from a single BP run should be treated cautiously without checking multiple azimuthal subsets or independent methods (e.g., empirical Green's function analysis, finite-fault inversion).

Fig. S1 in the Supplementary Information illustrates the back-projection average rupture directivity and aftershock migration for the 22 August 2025 Mw 7.5 and 10 October 2025 Mw 7.6 Drake Passage intraplate strike-slip doublet, in relation to inherited oceanic fracture-zone fabric.

Seismic data

The multichannel seismic line SA500-030 was acquired in the Austral summer 1987/1988 by the R/V "Almirante Camara" as part of the Brazilian Antarctic Program. The acquisition system used an array of 8 air-guns as the acoustic source (total volume 8.8 L), firing every 50 m, and a 1800 m-long

marine streamer with 72 channels as the recording system. The data are part of the Antarctic Seismic Data Library System (https://sdls.ogs.it), managed by the Istituto Nazionale di Oceanografia e di Geofisica Sperimentale (OGS) in Trieste (Italy), under the auspices of the Scientific Committee on Antarctic Research (SCAR). Processing steps applied to the data comprised: (1) spherical divergence and absorption compensation; (2) trace editing and despiking; (3) normal-move-out and common-depth-point stacks, using stacking velocities derived from semblance-velocity-analyses and constant-velocity-stacks (analysis performed every ~4 km); (4) deconvolution after stack; (5) time-variant filtering; and (6) Kirchhoff post-stack time migration.

Data availability

Regional earthquake catalogs are obtained from the International Seismological Centre – ISC (2026), On-line Bulletin, https://doi.org/10.31905/D808B830 and from the United States Geological Survey (USGS, Earthquake Hazards Program, 2017). Advanced National Seismic System (ANSS) Comprehensive Catalog of Earthquake Events and Products [Data set]. Global Centroid Moment Tensor (GCMT) solutions were retrieved from http://www.globalcmt.org. The seismological data of the Antarctic Seismographic Argentinean Italian Network (ASAIN), managed jointly by Italy's OGS and Argentina's IAA, are freely distributed via IRIS - https://ds.iris.edu/ds/nodes/dmc/services/seedlink/. The multichannel seismic profile SA500-030 presented in this study can be freely downloaded from the following URL: https://sdls.ogs.it/cache/index.jsp after registering and logging into the portal (in the query icon, digit the name of the line).

Code availability

The code used for template matching is available on Zenodo https://doi.org/10.5281/zenodo.7140418. P-wave back-projection rupture imaging is available at https://doi.org/10.17611/DP/BP.1. ObsPy package version 1.5 is used to download data (doi: 10.5281/zenodo.19005357). Software used for routine processing includes SeisComP (doi:10.5880/GFZ.2.4.2020.003). The processing of the seismic profile presented in this work was performed with the free, open-source software package SeismicUnix (SU).

Received: 22 April 2026; Accepted: 12 October 2026;
Published online: 30 October 2026

References

1. Robertson Maurice, S. D., Wiens, D. A., Shore, P. J., Vera, E. & Dorman, L. M. Seismicity and tectonics of the South Shetland Islands. *J. Geophys. Res.* **108**, 2465 (2003).
2. Parera-Portell, J. A., Mancilla, F. D. L., Almendros, J., Morales, J. & Stich, D. Slab tearing underneath the Bransfield Strait, Antarctica. *Geophys. Res. Lett.* **50**, e2023GL103813 (2023).
3. Eagles, G., Livermore, R. A. & Morris, P. Small basins in the Scotia Sea: the Eocene Drake Passage gateway. *Earth Planet. Sci. Lett.* **242**, 343–353 (2005).
4. Lodolo, E., Donda, F. & Tassone, A. Western Scotia Sea margins: improved constraints on the opening of the Drake Passage. *J. Geophys. Res.* **111**, B06101 (2006).
5. Maldonado, A. et al. A model of oceanic development by ridge jumping: opening of the Scotia Sea. *Glob. Planet. Change* **123**, 152–173 (2014).
6. van de Lagemaat et al. Subduction initiation in the Scotia Sea region and opening of the Drake Passage: when and why? *Earth Sci. Rev.* **215**, 103551 (2021).
7. Barker, P. F. The Cenozoic subduction history of the Pacific margin of the Antarctic Peninsula: Ridge crest–trench interactions. *J. Geol. Soc.* **139**, 787–801 (1982).
8. Eagles, G. Tectonic evolution of the Antarctic–Phoenix plate system since 15 Ma. *Earth Planet. Sci. Lett.* **217**, 97–109 (2004).
9. Choe, W. H., Lee, J. I., Lee, M. J., Hur, S. D. & Jin, Y. K. Origin of E-MORB in a fossil spreading center: the Antarctic-Phoenix Ridge, Drake Passage, Antarctica. *Geosci. J.* **11**, 185–199 (2007).
10. Livermore, R. et al. Autopsy on a dead spreading center: the Phoenix Ridge, Drake Passage, Antarctica. *Geology* **28**, 607–610 (2000).
11. Aldaya, F. & Maldonado, A. Tectonics of the triple junction at the southern end of the Shackleton Fracture Zone (Antarctic Peninsula). *Geo Mar. Lett.* **16**, 279–286 (1996).
12. Klepeis, K. A. & Lawver, L. A. Tectonics of the Antarctic-Scotia plate boundary near Elephant and Clarence Islands, West Antarctica. *J. Geophys. Res.* **101**, 20211–20231 (1996).
13. Kim, Y., Jin, Y. K. & Nam, S. H. Crustal structure of the Shackleton Fracture Zone in the southern Drake Passage, Antarctica. In *The Antarctic Region: Geological Evolution and Processes* Ricci, C. A. (Ed.) 661–667 (Tipologia Senense, 1997).
14. Geletti, R. et al. Seismic structure and tectonics of the Shackleton Fracture Zone (Drake Passage, Scotia Sea). *Mar. Geophys. Res.* **26**, 17–28 (2005).
15. Livermore, R., McAdoo, D. & Marks, K. Scotia Sea tectonics from high-resolution satellite gravity. *Earth Planet. Sci. Lett.* **123**, 255–268 (1994).
16. Maldonado, A. et al. Tectonics of an extinct ridge-transform intersection, Drake Passage (Antarctica). *Mar. Geophys. Res.* **21**, 43–68 (2000).
17. Pelayo, A. M. & Wiens, D. A. Seismotectonics and relative plate motions in the Scotia Sea region. *J. Geophys. Res.* **94**, 7293–7320 (1989).
18. Barker, P. F., Dalziel, I. W. D. & Storey, B. C. Tectonic development of the Scotia Arc region. In: Tingey, R. J. (eds.) *The geology of Antarctica*, 215–248 (Clarendon Press, 1991).
19. Christeson, G. L., Barker, D. H. N., Austin, J. A. Jr. & Dalziel, I. W. D. Deep crustal structure of Bransfield Strait: Initiation of a back arc basin by rift reactivation and propagation. *J. Geophys. Res.* **108**, 2492 (2003).
20. Catalán, M. et al. Initial stages of oceanic spreading in the Bransfield Rift from magnetic and gravity data analysis. *Tectonophysics* **585**, 102–112 (2013).
21. Dietrich, R. et al. ITRF coordinates and plate velocities from repeated GPS campaigns in Antarctica—An analysis based on different individual solutions. *J. Geod.* **74**, 756–766 (2001).
22. Thomas, C., Livermore, R. & Pollitz, F. Motion of the Scotia Sea plates. *Geophy. Journ. Intl.* **155**, 789–804 (2003).
23. Smalley Jr., R. et al. Scotia arc kinematics from GPS geodesy. *Geophys. Res. Lett.* **34** (2007).
24. DeMets, C., Gordon, R. G. & Argus, D. F. Geologically current plate motions. *Geoph. J. Intl.* **181**, 1–80 (2010).
25. Vuan, A. et al. The 2 May 2025 Mw 7.4 Drake Passage earthquake: insights into tectonics at the Shackleton Fracture Zone–Chilean Trench intersection. *ESS Open Archive* https://doi.org/10.22541/essoar.177082653.32028814/v1 (2026).
26. Bradley, K. & Hubbard, J. Another mid-M7 earthquake in the Drake Passage. *Earthq. Insights* https://doi.org/10.62481/385dcd37 (2025).
27. Plasencia et al. The Antarctic Seismographic Argentinean Italian Network (ASAIN): Recording Earthquakes in the Scotia Sea Region. *Seism. Soc. Am.* **92**, 748–2757 (2021).
28. Lay, T. & Kanamori, H. Earthquake doublets in the Solomon Islands. *Phys. Earth and Planet. Interiors* **21**, 283–304 (1980).
29. Ammon, C., Kanamori, H. & Lay, T. A great earthquake doublet and seismic stress transfer cycle in the central Kuril islands. *Nature* **451**, 561–565 (2008).
30. King, G. C. P., Stein, R. S. & Lin, J. Static stress changes and the triggering of earthquakes. *Bull. Seismol. Soc. Am.* **84**, 935–953 (1994).
31. Stein, R. The role of stress transfer in earthquake occurrence. *Nature* **402**, 605–609 (1999).
32. Wells, D. L. & Coppersmith, K. J. New empirical relationships among magnitude, rupture length, rupture width, rupture area, and surface displacement. *Bull. Seism. Soc. Am.* **84**, 974–1002 (1994).

33. Macario, A. et al. Flow line variations in abyssal hill morphology for the Antarctic Ridge at 65°S. *J. Geophys. Res.* **99**, 17,921–17,934 (1994).
34. Bohoyo, F. et al. Bathymetry and Geological Setting of the Drake Passage (1:1500000). *BAS GEOMAP 2 series*, Sheet 7, British Antarctic Survey, Cambridge, UK (2016).
35. Jin, Y. K., Lee, J., Hong, J. K. & Nam, S. H. Is subduction ongoing in the South Shetland Trench, Antarctic Peninsula? New constraints from crustal structures of outer trench wall. *Geosci. J.* **13**, 59–67 (2009).
36. Govers, R. & Wortel, M. J. R. Lithosphere tearing at STEP faults: Response to edges of subduction zones. *Earth Planet. Sci. Lett.* **236**, 505–523 (2005).
37. Faccenna, C. et al. Subduction dynamics, mantle flow, and slab tearing. *Tectonics* **36**, 171–192 (2017).
38. Cesca, S. et al. Massive earthquake swarm driven by magmatic intrusion at the Bransfield Strait, Antarctica. *Commun. Earth Environ.* **3**, 89 (2022).
39. Parera-Portell, J. A., Mancilla, F. D. L., Morales, J., Almendros, J. & Jimenez-Morales, V. Structure of the crust and upper mantle beneath the Bransfield Strait (Antarctica) using P receiver functions. *Tectonophysics* **802**, 228744 (2021).
40. Espinoza Celi, J. A., Cahuana-Yánez, N. G., Martillo-Bustamante, C. E. & González-Bonilla, M. Bransfield Strait and South Shetland Islands sedimentary basement and upper crustal structure: an analysis of gravity and magnetic data at the northwestern area of the Antarctic Peninsula. *Tectonophysics* **852**, 229771 (2023).
41. Galindo-Zaldívar, J., Gamboa, L., Maldonado, A., Nakao, S. & Bochu, Y. Tectonic development of the Bransfield Basin and its prolongation to the South Scotia Ridge, northern Antarctic Peninsula. *Mar. Geol.* **206**, 267–282 (2004).
42. Lodolo, E. & Pérez, L. F. An abandoned rift in the southwestern part of the South Scotia Ridge (Antarctica): implications for the genesis of the Bransfield Strait. *Tectonics* **34**, 2451–2464 (2015).
43. Wiens, D. A., Wysession, M. E. & Lawver, L. Recent oceanic intraplate earthquake in balleny sea was largest ever detected. *EOS* **79**, 351–353 (1998).
44. Antolik, M., Kaverina, A. & Dreger, D. S. Compound rupture of the great 1998 Antarctic plate earthquake. *J. Geophys. Res.* **105**, 23825–23838 (2000).
45. Henry, C., Das, S. & Woodhouse, J. H. The great March 25, 1998, Antarctic Plate earthquake: moment tensor and rupture history. *J. Geophys. Res*. **105**, 16097–16118 (2000).
46. Weinstein, Y., Nuriel, P., Inbar, M., Jicha, B. R. & Weinberger, R. Impact of the Dead Sea Transform kinematics on adjacent volcanic activity. *Tectonics* **39**, e2019TC005645 (2020).
47. Haddad, A. et al. Rifting-driven magmatism along the Dead Sea continental transform fault. *Geoph. Res. Lett.* **50**, e2022GL099964 (2023).
48. Polonia, A. et al. The ionian and alfeo-etna fault zones: new segments of an evolving plate boundary in the central Mediterranean Sea? *Tectonophysics* **675**, 69–90 (2016).
49. Polonia, A. et al. Lower plate serpentinite diapirism in the Calabrian Arc subduction complex. *Nat. Commun.* **8**, 2172 (2017).
50. Woollam, J. et al. SeisBench—A toolbox for machine learning in seismology. *Seism. Res. Lett.* **93**, 1695–1709 (2022).
51. Vuan, A., Sugan, M., Amati, G. & Kato, A. Improving the detection of low-magnitude seismicity preceding the Mw 6.3 L'Aquila earthquake: development of a scalable code based on the cross correlation of template earthquakes. *Bull. Seismol. Soc. Am.* **108**, 471–480 (2018).
52. Ishii, M., Shearer, P. M., Houston, H. & Vidale, J. E. Extent, duration and speed of the 2004 Sumatra–Andaman earthquake imaged by the Hi-Net array. *Nature* **435**, 933–936 (2005).
53. Xu, Y., Koper, K. D., Sufri, O., Zhu, L. & Hutko, A. R. Rupture imaging of the Mw 7.9 12 May 2008 Wenchuan earthquake from back projection of teleseismic P waves. *Geochem. Geophys. Geosyst.* **10**, Q04006 (2009).
54. Koper, K. D., Hutko, A. R., Lay, T. & Sufri, O. Imaging short-period seismic radiation from the 27 February 2010 Chile (Mw 8.8) earthquake by back-projection of P, PP, and PKIKP waves. *J. Geoph. Res.* **117**, B02308 (2012).
55. Vuan, A., Sugan, M. & Plasencia Linares, M. P. A reappraisal of surface wave group velocity tomography in the Subantarctic Scotia Sea and surrounding ridges. *Global Planet. Change* **123**, 223–238 (2014).

Acknowledgements

Seismological data were provided by the Antarctic Seismographic Argentinean Italian Network (ASAIN) and the International Seismological Centre (ISC). Earthquake data from the Unites States Geological Survey (USGS) were obtained from https://earthquake.usgs.gov/earthquakes/search/. The authors acknowledge the scientific and logistical support of Dirección Nacional del Antártico (DNA) – Instituto Antártico Argentino (IAA) and the essential role of the personnel of the Armada, Ejército, and Fuerza Aérea Argentina in maintaining the operating conditions for the ASAIN stations at the Antarctic bases. We thank Luiz Gamboa, the scientific coordinator of the campaign during which the seismic line presented in this work was acquired. We also thank Milton Plasencia Linares and Alessio Compagno for facilitating the distribution of the JUBA station data.

Author contributions

E.L.: Conceptualization, methodology, visualization, writing–original draft. A.V.: Formal analysis, data curation, validation, writing–review and editing. A.P.: Formal analysis, writing–review and editing. M.M.: Formal analysis, writing–review and editing. A.M.: Formal analysis and data curation. M.S.: Formal analysis and data curation.

Funding

No funding for this work.

Competing interests

The authors declare no competing interests.

Additional information

Supplementary information The online version contains supplementary material available at https://doi.org/10.1038/s43247-026-04197-1.

Correspondence and requests for materials should be addressed to Emanuele Lodolo.

Peer review information *Communications Earth & Environment* thanks all reviewer(s) for their contribution to the peer review of this work. Primary handling editor: Nikita Kaushal. A peer review file is available.

Reprints and permissions information is available at http://www.nature.com/reprints

Publisher's note Springer Nature remains neutral with regard to jurisdictional claims in published maps and institutional affiliations.

Open Access This article is licensed under a Creative Commons Attribution-NonCommercial-NoDerivatives 4.0 International License, which permits any non-commercial use, sharing, distribution and reproduction in any medium or format, as long as you give appropriate credit to the original author(s) and the source, provide a link to the Creative Commons licence, and indicate if you modified the licensed material. You do not have permission under this licence to share adapted material derived from this article or parts of it. The images or other third party material in this article are included in the article's Creative Commons licence, unless indicated otherwise in a credit line to the material. If material is not included in the article's Creative Commons licence and your intended use is not permitted by statutory regulation or exceeds the permitted use, you will need to obtain permission directly from the copyright holder. To view a copy of this licence, visit http://creativecommons.org/licenses/by-nc-nd/4.0/.

© The Author(s) 2026

This Article in Press is shared early to give you faster access to new research. It is citable and carries a permanent DOI. The final edited version will replace it automatically.